RF–DRIVER LINEAR COLLIDERS*

P. B. WILSON

Stanford Linear Accelerator Center
Stanford University, Stanford, California 94305

Summary

The next generation of linear collider after the SLC (Stanford Linear Collider) will probably have an energy in the range 300 GeV–1 TeV per linac. A number of exotic accelerating schemes, such as laser and plasma acceleration, have been proposed for linear colliders of the far future. However, the technology which is most mature and which could lead to a collider in the above energy range in the relatively near future is the rf-driven linac, in which externally produced rf is fed into a more or less conventional metallic accelerating structure. Two basic technologies have been proposed for producing the required high peak rf power: discrete microwave power sources, and various two-beam acceleration schemes in which the rf is produced by a high current driving beam running parallel to the main accelerator. The current status of experimental and analytic work on both the discrete source and the two-beam methods for producing rf are discussed. The implications of beam-beam related effects (luminosity, disruption and beamstrahlung) for the design of rf-driven linear colliders are also considered.

1. Elements of a Linear Collider

A conceptual diagram showing the principle elements of a linear collider is given in Fig. 1. Referring to systems as indicated in the figure:

A One of the injector liners must produce positrons.

B The damping rings must store and damp bunches to a very low normalized emittance.

C The preaccelerator may operate at a lower frequency than the main linac in order to reduce emittance growth at low energy where wakefield effects are most critical.

D The accelerating structure must provide a high accelerating gradient per unit of stored electromagnetic energy, without producing intolerable wakefield effects.

E The focussing lattice is also important in defining the beam dynamics of the main linac.

F The driver must supply electromagnetic energy in an appropriate form to the accelerating structure. The conversion of "wallplug" power to electromagnetic energy must be carried out with good efficiency.

G The final focus system must focus the accelerated beams to submicron transverse dimensions at the interaction point.

H The raison d'etre for a linear collider is the particle production that takes place when the bunches collide at the interaction point. The intense fields in the colliding bunches also produce beam-beam effects such as disruption and beamstrahlung, which couple strongly to the collider design.

Table 1

Accelerator Type	Driver	Structure
RF linac	Microwave tubes	Periodic copper guide
Two beam accelerator	High current parallel beam and transfer structures	Periodic copper guide
Wakefield accelerator	Concentric ring beam	Radial line Transformer
Switched power accelerator	Concentric switches	Radial line transformer
Plasma wakefield accelerator	Electron beam	Plasma
Laser beatwave accelerator	Laser	Plasma

Some possible driver-structure combinations are shown in Table 1. For the first two examples, rf is produced externally and fed into copper accelerating structures at discrete feed points. For the other examples, the electromagnetic energy which provides the accelerating field is generated in the structure itself. Deflecting fields produced by the driver are then generally comparable to the longitudinal accelerating field and strongly affect the beam if asymmetries are present.

The maturity of the various technologies listed in Table 1 is also an important consideration. A linear collider built within the next decade will almost certainly be based on a more or less conventional linac structure powered by externally produced rf. The design of the such a rf-driven linear collider is the focus of this paper.

2. Review of Beam–Beam Effects

2.1 Luminosity

The bottom line of a linear collider design is the luminosity, given for the head-on collision of two gaussian bunches by

$$L_1 = N^2 f_r H_D / 4\pi A \quad , \tag{2.1}$$

where N is the number of particles per bunch, H_D is the pinch enhancement factor (see the next section), f_r is the bunch collision rate and $A = \sigma_x \sigma_y$ is the beam area. The area is in turn related to the vertical and horizontal normalized emittances ϵ_{nx} and ϵ_{ny} by

$$A = \left(\epsilon_{nx}\epsilon_{ny}\beta_x^*\beta_y^*\right)^{1/2}/\gamma \quad , \tag{2.2}$$

where γ is the ratio of electron energy to rest energy and β_x^* and β_y^* are the beta functions at the collision point. If a single bunch is accelerated during each linac pulse, then f_r is also

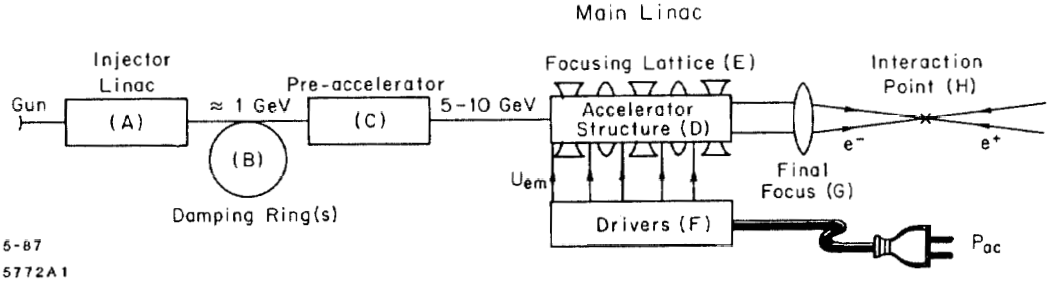

Figure 1. Conceptual diagram of a linear collider.

* Work supported by the Department of Energy, contract DE-AC03-76SF00515.

CH2387-9/87/0000-0053 $1.00 © IEEE
PAC 1987

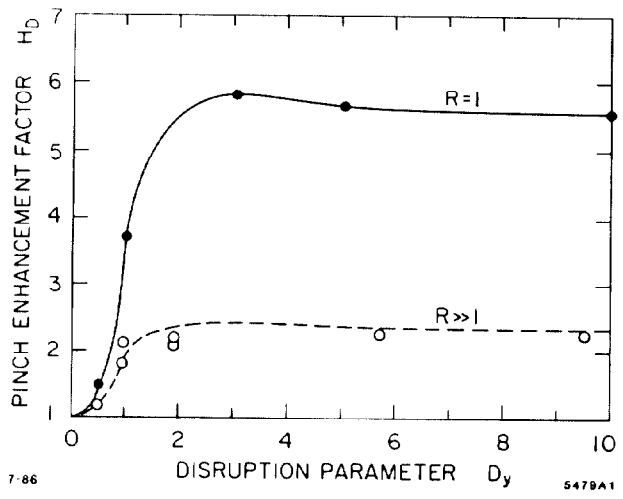

Figure 2. Pinch enhancement factor for colliding gaussian bunches. Points shown are from Ref. 2.

the linac repetition rate and the luminosity is the single bunch luminosity L_1. The situation is more complex if a train of b bunches is accelerated during each linac pulse. Several configurations are possible for colliding the bunch trains (see, for example, Ref. 1), leading to an enhancement in luminosity up to a maximum of bL_1 at a single collision point.

2.2 Disruption

When an electron bunch collides with a positron bunch, the collective fields from the particles in one oncoming bunch act like a lens to focus the particles in the other bunch toward the axis. For particles near the axis in a gaussian bunch the focal length of this lens is σ_z/D, where σ_z is the bunch length and D is the disruption parameter defined by

$$D = D_y = \frac{r_o N \sigma_z}{\gamma A}\left(\frac{2R}{1+R}\right) \quad . \tag{2.3}$$

Here $R = \sigma_x/\sigma_y \geq 1$ is the aspect ratio and $r_o = 2.82 \times 10^{-13}$ cm is the classical electron radius. Note that $D_x = D_y/R$, and that the disruption angles in the horizontal and vertical directions are equal,

$$\theta_{Dx} = \theta_{Dy} = \frac{2r_o N}{\gamma(\sigma_x + \sigma_y)} \quad . \tag{2.4}$$

If the disruption parameter is on the order of one, the bunches will pinch substantially as they pass through each other. This will reduce the effective transverse bunch area and enhance the luminosity. The enhancement factor H_D has been computed from simulations by Hollebeek[2] (see Fig. 2), Fawley and Lee[3], and Yakoya.[4] All of these simulations are in substantial agreement. If the pinch is not too large, the reduction in beam area can be computed using Eq. (2.4) to give

$$H_D(R, D_y) = \frac{RH_{D1}}{1 + (R-1)H_{D1}^{1/2}} \tag{2.5}$$

where $H_{D1} \equiv H_D(R = 1, D = D_y)$. For a very flat beam ($R \gg 1$), the enhancement factor at a given D_y is seen to approach the square root of the enhancement factor for a round beam with the same $D = Dy$. As shown in Fig. 2, this estimate is seen to be in reasonable agreement with simulation results, even for large values of the disruption where the calculation would not seem to apply.

2.3 Beamstrahlung

An electron or positron moving in the collective field of the oncoming beam emits synchrotron radiation, in this case called beamstrahlung. The energy radiated in time Δt by a single electron moving normally to an infinite, uniform magnetic field is

$$\Delta U = \frac{2r_o mc^3}{3\lambda_c^2}\Upsilon^2 H_\Upsilon \Delta t \quad , \tag{2.6}$$

where $\lambda_c = 3.86 \times 10^{-11}$ cm is the electron Compton wavelength divided by 2π. Here Υ is a scaling parameter defined by

$$\Upsilon \equiv \frac{2\hbar\omega_c}{3\gamma mc^2} = \frac{\gamma B}{B_c} \quad , \tag{2.7}$$

where $B_c = m^2c^3/e\hbar = 4.4 \times 10^{13} G$ and $\hbar\omega_c$ is the critical photon energy for classical synchrotron radiation. The function H_Υ describes the reduction in synchrotron radiation as the critical photon energy becomes comparable to, or exceeds, the electron energy γmc^2. Thus in the classical regime ($\Upsilon \ll 1$) the reduction factor approaches unity, while in the quantum regime ($\Upsilon \gg 1$) the reduction factor approaches[5] $H_\Upsilon \approx 0.556\Upsilon^{-4/3}$. The function $H_\Upsilon(\Upsilon)$ is plotted in Fig. 3.

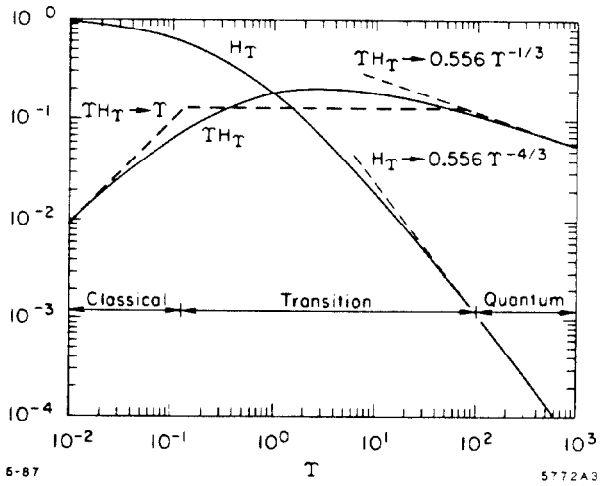

Figure 3. The beamstrahlung reduction factor H_Υ and the product ΥH_Υ as a function of the scaling parameter Υ.

If instead of a single particle moving in an infinite field we have a charge distribution moving through the nonuniform collective field of an oncoming bunch, the total radiation must be calculated by an appropriate integration of Eq. (2.6) over the bunch distributions. It turns out, perhaps rather surprisingly, that the total integrated radiation can be described by the single particle expression Eq. (2.6) provided an effective upsilon, $\bar{\Upsilon}$, is specified in terms of the bunch parameters,

$$\bar{\Upsilon} = \frac{F_\Upsilon r_o \lambda_c \gamma N}{\sigma_z A^{1/2}}\left[\frac{2R^{1/2}}{1+R}\right] \quad , \tag{2.8}$$

and an effective radiation time by $\Delta t = F_t \sigma_z/c$. The form factors F_Υ and F_t, as determined by analytic calculations[6] for gaussian bunches in the classical and extreme quantum regimes, are $F_\Upsilon = 0.41$ and $F_t = 1.93$. These factors also give agreement with simulations[4,5] for both round and flat beams in both regimes.

In the classical limit Eqs. (2.6) and (2.8), together with $\Delta t = 1.93\sigma_z/c$, give (assuming no pinch) the classical beamstrahlung energy loss

$$\delta_{cl} \equiv \frac{\Delta U}{\gamma mc^2} = \frac{0.22 r_o^3 \gamma N^2}{\sigma_z A}\left[\frac{4R}{(1+R)^2}\right] \quad . \tag{2.9a}$$

Beamstrahlung in the general case is then given by

$$\delta = \delta_{cl} H_\Upsilon(\bar{\Upsilon}) \quad . \tag{2.9b}$$

In the presence of pinch, the bremstrahlung as well as the luminosity is enchanced by a reduction in the effective bunch area. The effect on $\bar{\Upsilon}$ can be estimated by replacing the expression in brackets in Eq.(2.8) by

$$f(R, D_y) = \frac{2(H_{D1}R)^{1/2}}{2 + H_{D1}^{1/2}(R-1)} \quad , \tag{2.10}$$

where again H_{D1} is the round beam enhancement factor evaluated at the flat beam value of D_y. In the expression for classical beamstrahlung, Eq. (2.9a), the factor in brackets is replaced by $[f(R, D_y)]^2$.

By eliminating σ_z and N^2/A in Eq. (2.9) using Eqs. (2.1) and (2.8), we obtain

$$\delta \approx 40\bar{\Upsilon} H_\Upsilon \left\{\frac{L_1(10^{32} cm^{-2} s^{-1})}{f_r(Hz)}\right\}^{1/2}\left[\frac{2R^{1/2}}{1+R}\right] \quad . \tag{2.11}$$

Thus, if the luminosity is fixed, the beamstrahlung depends only on the repetition rate and the function $\bar{\Upsilon}H_\Upsilon$, plotted in Fig. 3. It is seen that, depending on $\bar{\Upsilon}H_\Upsilon$, the beamstrahlung falls into roughly three regimes:

Classical $(\bar{\Upsilon} < 0.1)$

$$\delta \approx 40\bar{\Upsilon}\left[\frac{L_1(10^{32})}{f_r}\right]^{1/2}\left(\frac{2R^{1/2}}{1+R}\right) \tag{2.12a}$$

Transition $(0.1 < \bar{\Upsilon} < 100)$

$$\delta \approx 5\left[\frac{L_1(10^{32})}{f_r}\right]^{1/2}\left(\frac{2R^{1/2}}{1+R}\right) \tag{2.12b}$$

Quantum $(\bar{\Upsilon} > 100)$

$$\delta \approx 20\bar{\Upsilon}^{-1/3}\left[\frac{L_1(10^{32})}{f_r}\right]^{1/2}\left(\frac{2R^{1/2}}{1+R}\right) \tag{2.12c}$$

Here L_1 is in units of 10^{32} cm^{-2} s^{-1}. Expression (2.12b) is of major importance, because all parameter lists suggested so far for the next generation of linear colliders (300 GeV to 1 TeV per linac) lead to values for $\bar{\Upsilon}$ in this range. This will be shown in the following section using a useful expression for $\bar{\Upsilon}$ obtained by eliminating N^2/A using Eqs. (2.1) and (2.8):

$$\bar{\Upsilon} \approx 3.3\left\{\frac{[E_o(\mathrm{TeV}]\,[L_1(10^{32})]^{1/2}}{[\sigma_z(mm)]\,[f_r(Hz)]^{1/2}}\right\}\left[\frac{2R^{1/2}}{1+R}\right] \quad . \tag{2.13}$$

Again, the function of R in the square brackets must be replaced by Eq. (2.10) if the bunches pinch due to disruption.

3. Peak and Average Power Requirements

3.1 Reference Collider Design

In the following sections we will refer to these parameters for a reference collider design:

Energy:	500 + 500 GeV (1 TeV c.m.)
Luminosity:	10^{33} cm^{-2} s^{-1} per bunch
Length:	3 + 3 km
Gradient:	167 MV/m
AC Power:	100 MW (both linacs)

3.2 Peak Power Requirement

The peak power per unit length required to reach an unloaded gradient G in a structure with elastance $s \equiv G^2/u$, where u is the stored energy per unit length, is

$$\frac{\hat{P}_{feed}}{L_s} = \frac{G^2}{\eta_s s T_f} \quad . \tag{3.2}$$

Here L_s is the structure length, $T_f = L_s/v_g$ is the filling time, $\hat{P}_{feed}$ is the peak power per feed and η_s is the structure efficiency (constant impedance traveling wave structure),

$$\eta_s = \left(\frac{1-e^{-\tau}}{\tau}\right)^2 \quad . \tag{3.2}$$

It is convenient to define the attenuation parameter τ in terms of the structure time constant $T_o = 2Q_o/\omega$ as $\tau = T_f/T_o$. The following table gives some sample parameters for a $2\pi/3$ mode constant impedance disk-loaded structure with $L_s = 1.0$ m operating at 11.42 GHz (four times SLAC frequency) and a gradient of 167 MV m. For structure details, see Ref. 7.

Table 2

Parameters	Disk Aperture Radius (cm) 0.37	0.43	0.50	Frequency Scaling
v_g/c	.030	.050	.074	Constant
T_f (ns)	112	67	45	$\omega^{-3/2}$
s $(\Omega/ps - m)$	1025	880	755	ω^2
T_o (ns)	195	197	198	$\omega^{-3/2}$
τ	0.58	0.34	0.23	Constant
η_s	0.58	0.72	0.80	Constant
$\hat{P}/L$ (MW/m)	420	660	1020	$\omega^{-1/2}$
$\hat{E}_{surface}/G$	2.2	2.35	2.5	Constant

The first structure in Table 2 has a relatively large attenuation parameter and filling time. The second and third structures have larger iris openings (and hence lower wakefields) and have filling times appropriate for induction linac technology.

The frequency scaling for various parameters is also indicated in Table 2, assuming fixed v_g/c and τ. In particular, the elastance for the first structure scales as

$$\begin{aligned} s &= s_o/\lambda^2 \\ s_o &= 0.706(\Omega - m)/ps \end{aligned} \quad . \tag{3.3}$$

3.3 Wall Plug Power

The average input ac power to the rf system of a collider of length L is given by

$$P_{ac} = \frac{f_r u L}{\eta_{rf}\eta_s} = \frac{f_r G V_o \lambda^2}{\eta_{rf}\eta_s s_o} \quad , \tag{3.4}$$

where V_o is the energy in volts and η_{rf} is the efficiency for conversion of "wall plug" power to rf at the input to the structure.

Using values of s_o and η_s for the first structure in Table 2, and assuming also a net rf conversion efficiency of 50%, Eq. (3.4) becomes

$$P_{ac}(W) = 4.9 \times 10^{-12} f_r(Hz) V_o(V) G(V/m) \lambda^2(m) \quad . \quad (3.5)$$

Using the reference design parameters, we can compute the repetition rate as a function of frequency, as shown in Table 3.

Table 3

Frequency (GHz)	Wavelength (cm)	Rep. Rate (Hz)	Beamstrahlung R=1	R=10	R=100
2.856 (SLAC)	10.5	11	(4.8)	(2.7)	(1.0)
11.42 (4x SLAC)	2.63	180	(1.2)	(0.7)	0.24
17.14 (6x SLAC)	1.75	400	(0.8)	0.45	0.16
30	1.0	1200	0.45	0.26	0.09

Next, use Eq. (3.5) to eliminate f_r in (2.13) to obtain

$$\bar{\Upsilon} \approx 7.2 \times 10^{-3} \left\{ \frac{[E_o(TeV)]^{3/2} \left[L_1(10^{32})\right]^{1/2} [G(MV/m)]^{1/2}}{(\sigma_z/\lambda) [P_{ac}(MW)]^{1/2}} \right\} \times \left[2R^{1/2}/(1+R)\right] \quad (3.6)$$

Note $E_o = eV_o$ and P_{ac} are per linac. For our reference collider parameters we obtain

$$(\sigma_z/\lambda)\bar{\Upsilon} = .015 \left[2R^{1/2}/(1+R)\right] \quad . \quad (3.7)$$

Thus, for a round beam in the classical beamstrahlung regime ($\bar{\Upsilon} < 0.1$) we must have $\sigma_z/\lambda > 0.15$, while $\sigma_z/\lambda < 1.5 \times 10^{-4}$ in the quantum regime ($\bar{\Upsilon} > 100$). For a flat beam ($R = 100$) the corresponding values are $\sigma_z/\lambda > 0.03$ (classical) and $\sigma_z/\lambda < 3 \times 10^{-5}$ (quantum). For wavelengths of a few centimeters, the required bunch lengths are unreasonably long for the classical case and unreasonably short for the quantum case.

We conclude that the next generation of linac collider will operate in the transition regime with $0.1 < \Upsilon < 100$, and that Eq. (2.12b) can be used to estimate the beamstrahlung parameter. The last three columns in Table III give δ using this expression for the repetition rates shown, assuming also the reference luminosity of 10^{33} cm^{-2} s^{-1} per bunch. The values in parentheses are meaningless, since the beamstrahlung expressions were derived assuming that the beamstrahlung loss is small compared to the initial electron energy. Viable cases are underlined. The conclusion to be drawn is that, given reasonable constraints on the allowable beamstrahlung and wall plug power, the rf frequency for the next generation collider will be on the order of 10 GHz or higher. The frequency will be limited to perhaps 30 GHz at the upper end by other difficulties, such as wakefield effects, peak power limitations on rf sources and the complexity and cost of the associated rf technology.

4. RF Power Sources

4.1 Microwave Tubes

In Table 2 we note that a peak power of 420 MW is required for each 1.0 m structure operating at a gradient of 167 MV/m with a filling time of 112 ns. Assume discrete rf power sources with a pulse length of 0.9 μs, together with rf pulse compression by a factor of 8 with an efficiency of 80% (see Section 4.5). The required peak source power is then 65 MW if there is one source per meter (one per structure feed) and 130 MW for sources spaced 2 m apart. Several types of rf sources are possible candidates for power production at this level.

Klystrons. A klystron operating at 2.856 GHz and $T_p = 1.0$ μs has delivered a peak power of 150 MW.[8] If this tube design is scaled up by a factor of 4 in frequency to 11.42 GHz, it might achieve a peak power on the order 10 MW. To reach a peak power level of 100 MW in a conventional round-beam klystron design, a higher beam voltage will almost certainly be required. At SLAC a klystron design has been suggested[9] that would produce 100 MW at 8.57 GHz at a beam voltage of 540 kV.

High peak power can be achieved at a lower beam voltage if the beam area is increased, by making it either in the form of a linear sheet or a ring. A sheet beam klystron using periodic permanent magnet focusing on a beam 50 cm in length, which would deliver 100 MW at a voltage of 200 kV, is being studied[10] at SLAC. At somewhat higher voltages and beam convergence ratios, the same output power could be reached with a beam on the order of 15 cm in length. However, a serious problem that must be overcome in a tube of this type is feedback between cavities due to possible propogation of modes excited by mechanical errors.

An alternative klystron design also being studied[9] at SLAC would produce peak power at the required level without rf pulse compression. From Table 2 we note that the required power ranges from 660–1020 GW/m for filling times in the range 45–67 ns. These pulse lengths are a good match to the high power capability of the magnetic pulse compressors which drive induction linac modules.[11] The klystron voltage and current would be on the order of 1 MV and 1 kA.

Gyroklystrons. The transverse dimensions of the beam in a gyroklystron can exceed the rf wavelength. Consequently, these devices are capable of providing high peak and average power at very high frequencies. At the University of Maryland a gyroklystron capable of producing 30–50 MW at 10 GHz with a pulse length of 1.0 μs is being developed.[12] It is estimated that the power capability can be extended to the order of 300 MW by operating in a higher cavity radial mode.

4.2 Lasertrons

In the lasertron, rf current is created by illuminating a photocathode with a laser which is pulse modulated at the rf frequency. Thus, after acceleration by a high pulse or dc voltage, only a klystron-type output cavity is required to extract rf energy. In principle no modulator is needed; the voltage can be supplied by a simple (and presumably inexpensive) dc supply.

Work on lasertrons is in progress at several laboratories. At SLAC a lasertron is under development[13] which can provide 30–50 MW at 2.856 GHz. An active program of high power lasertron development is also underway in Japan[14] at a similar frequency. However, formidable technical problems remain to be overcome in order to demonstrate that the lasertron can be a reliable source of high peak power for a linear collider, especially at higher frequencies.

4.3 Two–Beam Accelerators

In the two-beam accelerator (TBA) a high current driving beam at relatively low energy runs parallel to the main accelerator. Along the driving beam transfer elements periodically extract rf energy, which is delivered through waveguides to the accelerating structures of the main accelerator. Interspersed with the transfer elements are reacceleration elements, which put energy back into the driving beam to keep its energy roughly constant.

Four proposed types of two-beam accelerators are listed in Table 4. In the first two examples the driving beam is bunched at the rf wavelength, and energy is extracted by an interaction with the longitudinal field in a cavity or section of slow wave structure (transfer cavity). In the second two examples, energy is extracted in a wiggler by the interaction of the beam with a transverse rf electric field. In both cases the driving beam can be reaccelerated by either induction modules or by superconducting rf cavities. Although design examples have been worked out in some detail for all four two-beam accelerator types, only an FEL driven by induction accelerator modules has so far produced high peak power (1.8 GW at 8 mm) in a TBA prototype experiment.[15]

Table 4

Drive Linac	Transfer Device	Reference
Induction Modules	Transfer cavities	A. M. Sessler and S. S. Yu[16]
Superconducting rf	Transfer cavities	W. Schnell[17]
Induction Modules	FEL	T. J. Orzechowski et al.[18]
Superconducting rf	FEL	Amaldi and Pellegrini[19]

4.4 Relativistic Klystrons

Induction accelerator technology can be conveniently packaged in units producing a 10 GW, 40–70 ns pulse (for example, the ARC accelerator[20] at LLNL). Such a pulse can be used to power a klystron with a very high beam voltage (on the order of 3 MeV). Such a device would probably consist of several bunching cavities (perhaps at ≈1 1/2 MV) and several output or transfer cavities to extract energy after acceleration to full voltage. The device resembles a short length of a two-beam accelerator, but it need not run parallel to the main accelerator. From Table 2 the required power per meter at 67 ns for the reference collider design is 660 MW. Thus, one such "relativistic klystron" would be capable of powering about 10 m of accelerator.

4.5 RF Pulse Compression

The details of an rf pulse compression scheme which can divide an input pulse length by a factor of 2^n, and increase the peak power by a factor of $2^n\eta_c(n)$, where η_c is the compression efficiency, are given in Ref. 21. The method depends only upon 180° phase shifters in the input drive to the high power amplifiers (klystrons), and on passive high power components (delay lines and 3 db couplers). The compression efficiency is determined by losses in the couplers and delay lines. Assuming the delay lines are 7.5 cm diameter round copper pipes operating in the TE_{01} mode at 11.42 GHz, and taking 0.2 db as the loss per coupler, then the compression efficiency and peak source power are given in Table 5. It is assumed that one source feeds two 1 m long accelerating sections operating at 167 MV/m.

Table 5

Number of Stages	Efficiencies Couplers	Lines	η_c	T_k (μs)	P_k (MW)
0	1.00	1.00	1.00	0.112	840
1	0.955	0.99	0.945	0.225	445
2	0.91	0.97	0.88	0.45	240
3	0.87	0.92	0.80	0.9	130
4	0.83	0.835	0.69	1.8	75

5. Accelerating Structures

5.1 RF Breakdown Limits

Table 6 summarizes recent experimental results[22] on rf breakdown in disk-loaded structures. The results were obtained for pulse lengths of $1\frac{1}{2}$–3 μs. Note that the breakdown field scales as $E_b \approx \omega^{1/2}$. The variation with pulse length T_p was not measured, but there is some experimental evidence for $E_b \sim T_p^{-1/4}$ for short pulse lengths. For a filling time which varies as $\omega^{-3/2}$, the net scaling is then $E_b \sim \omega^{7/8}$. The operating gradient may need to be considerably lower than shown because of intense field emission current near the breakdown limit.

Table 6

Frequency (GHz)	Surface $\hat{E}_s$ (MV/m)	Gradient at $\hat{E}_s/G = 2.2$ (MV/m)
2.856	318	145
5.7	445	202
9.3	572	260

5.2 Disk-Loaded Structures

Figure 4 shows the variation of the elastance s, peak surface field to gradient ratio $\hat{E}_s/G$, internal time constant T_o and disk aperture radius a as a function of group velocity for a SLAC-type $2\pi/3$ mode disk-loaded structure. This well-documented structure serves as a standard against which more exotic structure ideas can be compared.

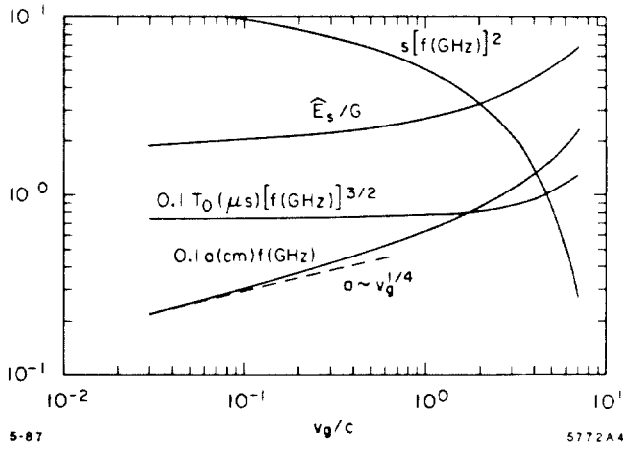

Figure 4. Properties of a $2\pi/3$–mode disk-loaded structure (disk thickness 0.056 λ) as a function of group velocity

5.3 Novel Structures

A useful concept in comparing accelerating structures is the energy confinement radius, r_c, defined in terms of the stored energy per unit length by $u = \pi r_c^2 \epsilon_o G^2 = G^2\lambda^2/s_o$. For a disk-loaded structure at $v_g/c = .03, r_c/\lambda = 0.23$ and $r_c/a = 1.61$. Thus for this case the stored energy is reasonably well confined to the beam aperture, and there is not much hope for finding another structure with a significant improvement in elastance at a given wavelength. However, to reduce wakefield effects in a linear collider, it would still be desirable to open up the beam aperture compared to that for a disk-loaded structure, if this can be done without degrading the elastance significantly.

A number of novel structures with relatively large a/λ ratios are discussed in Ref. 7. Several structures with bellows-like wall corrugations give values for s and a/λ which are comparable to those for a disk-loaded structure at the same group velocity. They have the advantage that they might be easier to fabricate, although the elastances tend to be low because the group velocity is high ($v_g/c > 0.1$). However, one novel structure, the undulating waveguide structure, has a beam aperture about $2\frac{1}{2}$ times that of a disk-loaded structure at the same wavelength. The elastance, however, is down by about the same factor. Since the structure also has a higher Q_o, the filling time can be longer and the peak power requirement would be about the same as that for a disk-loaded structure.

6. Putting It All Together

In this collider design exercise, we have assumed that the parameters of $L, \gamma, \delta_{bs}, P_{ac}$ and G have been specified *a priori*. From technology considerations, together with Table 3, we pick an operating frequency which then fixes the repetition rate and beam aspect ratio. From Eqs. (2.11) and (2.13) $\bar{\Upsilon}, \sigma_z$ and N^2/A are now fixed. We next pick a value for N which gives reasonable values for disruption, beam area and beam efficiency using the following expressions:

$$DH_D = 1.0 \times 10^9 \left\{ \frac{\delta^3}{\bar{\Upsilon}^4 H_\Upsilon^3 N} \right\} \left[\frac{1+R}{2} \right] \tag{6.1}$$

$$A^{1/2}(\mu m) = 1.1 \times 10^{-11} \left\{ \frac{H_D^{1/2} \bar{\Upsilon} H_\Upsilon N}{\delta} \right\} \left[\frac{2R^{1/2}}{1+R} \right] \tag{6.2}$$

$$\eta_b = \frac{e s_o N}{G \lambda^2} \quad . \tag{6.3}$$

N should be large enought to give $D \lesssim 10$ and to keep the beam area from becoming unreasonably small. From Eq. (2.2) the minimum beam area is determined by the minimum normalized emittance that can be produced by a reasonable damping ring design, and by the minimum $\beta_x^* \beta_y^*$ that can be produced in a reasonable final focus system. This is of course a long and complex story, but *very* roughly we can say[23]

$$(\epsilon_{nx} \epsilon_{ny})^{1/2}_{\min} \approx 5 \times 10^{-7} \mathrm{m-rad}$$

$$(\beta_x^* \beta_y^*)^{1/2}_{\min} \approx 1 \text{ mm} \quad ,$$

giving $A^{1/2}_{\min} \approx 0.02$ μm for 500 GeV beams. To achieve the above β^*, the energy spread must be very small ($\approx 2 \times 10^{-3}$), since $\beta_y^* \sim \sigma_p^2$. The energy spread is determined largely by the longitudinal wake. For a given accelerating structure, $\sigma_p = f(\eta_b, \sigma_z/\lambda)$. The method for calculating the wake-induced energy spread, and examples for the SLAC structure, are given in Ref. 24.

Transverse emittance growth due to dipole wakefields[25] and chromatic effects[26] in the linac must also be limited in a viable collider design. The transverse wake depends strongly on the beam aperture; for example, it varies roughly as $W_\perp \sim \sigma_z/a^{3.5}$ in a disk-loaded structure. Structures, such as the underlating waveguide structure mentioned in Section 4.3, have been suggested which have no transverse wake in one transverse direction and a greatly reduced wake in the other.

In summary, we have seen that the parameters of a linear collider are interrelated by a complex web of constraints. R. Palmer[23] has developed a computer program based on approximate expressions for these interdependent relationships. His results lead to some (still preliminary) conclusions: (1) Using short bunches (≈ 30 μm) and flat beams (R ≈ 100) intersecting at an angle, a luminosity on the order of 1×10^{33} per bunch is possible for the reference collider parameters of Section 3.1 at rf frequencies in the range of 10–30 GHz. (2) Colliding multiple bunches per fill would give 5–10 times more luminosity, if long range transverse wake effects can be controlled. (3) However, a factor of 5–10 degradation in luminosity is also likely due to emittance growth and collision jitter.

References

1. P. B. Wilson, *Proceedings of the 1986 Linear Accelerator Conference,* SLAC–303 (1986), p. 585.
2. R. Hollebeek and A. Minton, SLAC Internal Note CN–302 (1985).
3. W. M. Fawley and E. P. Lee, private communication.
4. Kaoru Yokoya, KEK Report 85–9 (1985).
5. For details see, for example, R. Noble, SLAC–PUB–3871 (1986).
6. Kaoru Yokoya, Nucl. Instrum. Methods **A251,** 1 (1986).
7. Z. D. Farkas and P. B. Wilson, this conference. Also SLAC–PUB–4088 (1987).
8. T. G. Lee et al., SLAC–PUB–3619 ('1985).
9. M. A. Allen, private communication.
10. K. R. Eppley, W. B. Herrmannsfeldt and R. H. Miller, this conference. Also SLAC–PUB–4221 (1987).
11. See, for example, LLL–TB–63, Lawrence Livermore National Laboratory (1984).
12. V. L. Granatstein et al., to be published in Proceedings SPIE Technical Symposium Southeast, Orlando, Florida, May 1987.
13. C. K. Sinclair, SLAC–PUB–4111 (1986).
14. Y. Fukushima et al., Nucl. Instrum. Methods **A238,** 215 (1985).
15. A. M. Sessler and D. Vaughan, Am. Scientist **75,** 35 (1987).
16. A. M. Sessler and S. S. Yu, UCRL–96083 (1987); submitted to Phys. Rev. Lett.
17. W. Schnell, CERN–LEP–RF/86–06 and CERN–LEP–RF/86–27.
18. T. J. Orzechowski et al., UCRL–91931 (1984); submitted to IEEE J. Quantum Electronics.
19. U. Amaldi and C. Pellegrini, CERN Internal Note CLIC–16 (1986).
20. D. L. Birx, private communication.
21. Z. D. Farkas, *IEEE Trans. Microwave Theory and Techniques,* **MTT–34,** 1036 (1986). Also SLAC–PUB–3694.
22. G. A. Loew, private communication.
23. See, for example, R. Palmer, SLAC–PUB–4295 (1987).
24. See, for example, P. B. Wilson, SLAC–PUB–2884, Sec. 10.1 (1982).
25. Karl L. F. Bane, SLAC–PUB–4169 (1986).
26. R. Ruth, private communication.